



## Advancing Interceptor Design: Analyzing the Impact of Extended Stern Form on Deep-V Planing Hulls

Samuel<sup>1,\*</sup>, Rizal Kurnia Praja<sup>1</sup>, Deddy Chrismianto<sup>1</sup>, Muhammad Luqman Hakim<sup>1</sup>, Ahmad Fitriadhy<sup>2</sup>, Aldias Bahatmaka<sup>3</sup>

<sup>1</sup> Department of Naval Architecture, Faculty of Engineering, Diponegoro University, Jl. Prof. Soedarto, S.H, Tembalang, Semarang 50275, Indonesia

<sup>2</sup> Program of Maritime Technology, School of Ocean Engineering, Universiti Malaysia Terengganu, Malaysia

<sup>3</sup> Department of Mechanical Engineering, Universitas Negeri Semarang, Semarang, Indonesia

### ARTICLE INFO

#### Article history:

Received 20 July 2023

Received in revised form 23 August 2023

Accepted 19 September 2023

Available online 3 January 2024

#### Keywords:

Drag; Interceptor; Extended Stern; Planing Hull; CFD; Boundary Layer

### ABSTRACT

The deep-v planing hull is designed to operate at high speeds because most of the hull's weight is supported by the hydrodynamic lift acting on the hull base. Planing hull form characteristics such as deadrise angle, chines, and extended stern significantly affect the ship's hydrodynamic performance. The addition of the interceptor is an innovation to reduce the total resistance of the ship by controlling the trim angle. However, the form of the ship's stern is not always the same; thus, it needs to be studied based on the form of the ship's stern. The extended stern form refers to modifying the hull geometry at the rear, particularly the stern extension beyond its conventional length. This research aimed to analyze the hydrodynamic performance of the interceptor at the extended stern angle. Furthermore, Computational Fluid Dynamics (CFD) simulations were performed to analyze the effect of the extended stern form. A numerical model of the deep-V planing hull with variations of the stern extension was developed, and the flow behavior around the hull was analyzed using CFD techniques. Simulations were conducted under various operating conditions, including different speeds and interceptor strokes. The results indicated that the extended stern's different forms could affect the ship's resistance, trim, and heave. The reduction in resistance was seen at moderate speeds, thereby reducing steep trim angles. The greater the extended stern angle, the more significant the reduction in ship resistance at  $Fr$  0.58 by 26%. Likewise, the combination of interceptor and extended stern experienced a decrease in resistance in the semi-displacement phase with a percentage of 33% resistance, 66% trim, and 47% heave. The interceptor stroke ( $d$ ) depended on the boundary layer ( $h$ ). The extended stern with angles of  $10^\circ$ ,  $20^\circ$ , and  $30^\circ$  were found to have  $d/h$  ratios of 0.38, 0.37, and 0.34. However, it should be noted that extending the stern without interceptors and with interceptors at high speeds could result in a dangerous increase in resistance on high-speed vessel.

\* Corresponding author.

E-mail address: [samuel@ft.undip.ac.id](mailto:samuel@ft.undip.ac.id) (Samuel)

<https://doi.org/10.37934/cfdl.16.5.5977>

## 1. Introduction

Boats with planing hulls continue to be developed with various innovations such as fast patrol boats, pilot ships, and Coast Guard patrol vessels [1]. In planing hull ships, most of the hull weight is supported by hydrodynamic lift acting on the hull base at high speeds; thus, it has excessive trim [2]. Reducing ship resistance is a ship architect's goal and a way to save energy. Some research had been carried out by modifying the hull and the propulsion system but it required much money.

Stern appendages such as the interceptor [3], trim tab [4], and Hydrofoil [5] serve to reduce resistance. The addition of an interceptor is an innovation on the ship's stern that has been studied extensively in recent years. The interceptor is a thin plate mounted perpendicular to the ship's stern. It increases pressure under the stern by blocking flow through the hull and reduces the trim angle by generating negative moments [3]. Tsai and Hwang conducted a model test to determine the effect of the stern flap, interceptor, and a combination of both on the planing hull of the ship. The integrated interceptor with a stern flap indicated more effective results in reducing resistance than using each appendage [4]. Furthermore, Day and Cooper studied the effects of using interceptors on sailing yachts. The interceptor showed a 10-18% reduction in resistance over a speed range of 8-20 knots [6].

Karimi *et al.*, [1] conducted trials on a catamaran planing hull model in calm and wavy water conditions. Applying an interceptor could reduce heave, pitch motion, and vertical acceleration. Researchers were increasingly exploring the interceptor because of its extraordinary advantages. Ghassemi *et al.*, [7] conducted tests on a planing hull with an interceptor. The result was high pressure generated between the interceptor and bottom, wet surface, and reduced resistance by the interceptor. Seok *et al.*, [3] discovered that the pressure at the bottom of the hull increased in proportion to the interceptor's speed and height for the interceptor's blocking effect. Suneela *et al.*, [8] considered that interceptor height played an essential role in ship performance. The installation location of the interceptor was also an essential factor, as illustrated by the test model by Karimi *et al.*, [10] the ship's resistance was clearly reduced by the interceptor located at the stern and midship, and the maximum resistance reduction for mono hull and catamaran ships were 15% and 12%, respectively. Sahin *et al.*, [9] revealed the best interceptor position between chine and the centerline, and the effect of interceptor height was directly related to ship speed. The magnitude of the lift created by the interceptor usually depended on the height and flow velocity. However, other parameters might affect the effectiveness of the interceptor [10].

Not all ships have a perpendicular stern form. Kim *et al.*, developed three hull models with the stern bottom of the VPS and VWC ships extended aft at 2.9 % LWL, while the VWS ships were at 4.3 % LWL. However, after being modified, there were no significant changes, and a porpoising phenomenon occurred at a speed of 30 knots. Adding an auxiliary device at the stern prevented the porpoising phenomenon [11]. As Mansoori *et al.*, [12] pointed out, the interceptor applied intense pressure aft of the ship. It also reduced the resistance and trim of the ship and increased the lift force coefficient, which directly affected the porpoising instability. According to the findings, the interceptor could entirely manage the porpoising issue.

Park *et al.*, [2] conducted research using the Aragon 2 hull form as a development of the three hulls using wave-controlled interceptors. As a result, pitch and heave could be reduced by 41.3% and 33.4%. According to studies on interceptors on regular waves, heave could be reduced by 16% to 18%. [13]. Interceptor research using the Aragon 2 hull form has also been carried out by Samuel *et al.*, with a 57% drag reduction in the close-to-chine position [14]. In other research with different interceptor forms, including the v-form interceptor, the result was a 21% drag reduced at a Froude number of 0.87 [15]. The choice of the optimal interceptor height greatly affected its efficiency [16].

The different forms of the stern certainly affected the effectiveness of the interceptor, such as the deadrise angle and variation of the stern's bottom, which was lengthened to reduce trim and resistance at high speeds.

Yousefi *et al.*, [17] revealed three CFD methods related to a planing hull, i.e., the Finite Element Method (FEM), Finite Volume Method (FVM), and Boundary Element Method (BEM). Due to its greater accuracy than other methods, FVM is the most popular method for predicting the planing hull characteristics. Sukas *et al.*, [18] conducted research using CFD, experimental, and empirical methods. They discovered that the CFD method with overset mesh could overcome the problem of flow at high speed around planing ships. Numerical simulation improved accuracy in resolving flows around the hull. Research using the overset mesh method had also been carried out by Fathuddin *et al.*, [19] which concluded that the overset mesh method had good accuracy in predicting resistance, trim, and heave of planing-type ships. Current advances in computer technology can create complex hydrodynamic force models and analyses. FVM-based numerical simulation methods are widely employed in interceptor analysis research. The RANS equation is used by the FVM approach to describe turbulent flow in both water and air.

Based on the background above, the interceptor is a tool to control trim; thus, the ship's resistance can be reduced at a certain speed. However, applying an interceptor with an extended stern form cannot be equated with a conventional ship. In this research, the interceptor would be simulated to obtain the ship's resistance at each speed. The approach to numerical simulations employed FVM based on RANS. The interceptor would generate a moment and change the pressure distribution at the ship's stern. CFD results would be verified with the experiment of Park *et al.*, [2] in calm water conditions. Section 2 provided an overview of the research procedures, and Section 3 provided various hydrodynamic characteristics such as resistance, trim, heave, lift force, and wave patterns as previously discussed.

## 2. Methodology

### 2.1 Research Object

This research used a Deep-V planing hull tested experimentally in calm water conditions with ITTC standards, Aragon 2 is the sixth generation hull development from Kim *et al.*, [20]. The ship, designed without passengers, was built on a full scale by the Korea Research Institute of Ships and Ocean Engineering (KRISO) for military purposes. Turning characteristic testing was carried out by Kim *et al.*, [21]. Park *et al.*, [2] conducted subsequent research by integrating the interceptor. The Aragon 2 CAD model is illustrated in Figure 1, and the main dimension can be seen in Table 1.

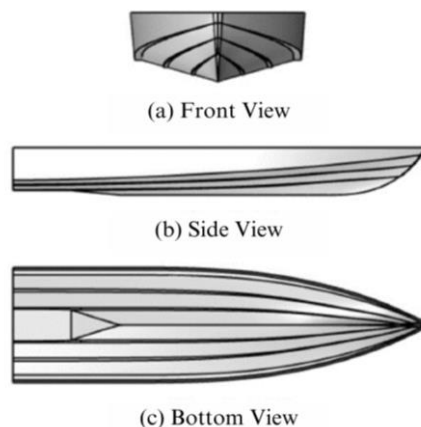


**Fig. 1.** Aragon 2 hull form

**Table 1**  
 Main dimension

Dimension	Full scale	Model scale	Unit
Scale	1	5.33	
LOA	8.00	1.50	Meter
LWL	7.53	1.41	Meter
B	2.20	0.41	Meter
T	0.42	0.08	Meter
$\Delta$	3000	19.78	Kg

## 2.2 Research Object

This research aims to analyze the ship's drag, trim, and heave due to the interceptor on the different forms of the extended stern. The interceptor used was the Humphree X300 interceptor with a span(s) width of 300 mm and a stroke height (d) of 50 mm [22]. The extended stern's bottom was a modification to the ship stern to reduce the total resistance of the ship, trim angle, and the power needed at high speeds; hence, it could improve ship performance [11]. The variations of the research model are shown in Table 2. Furthermore, the visualization of the extended stern and the installation of the interceptors are shown in Figures 2 and 3, as well as the variations in the height of the interceptor in Figure 4.

**Table 2**  
 Model variation

Parameter	Variable
Extended stern	10°, 20°, 30°
Interceptor height	20%, 60%, 100%
Froude number	0.29; 0.58; 0.87; 1.16; 1.45

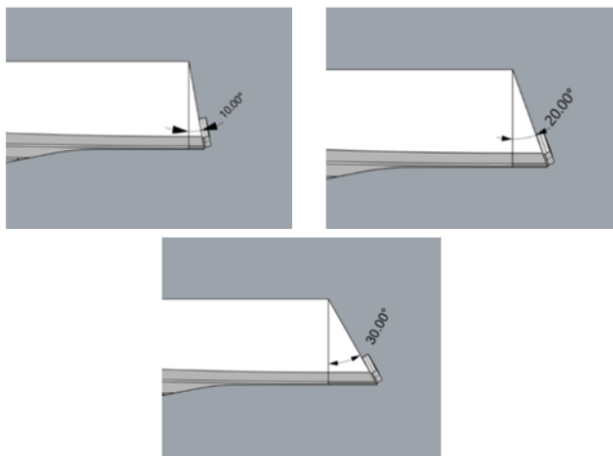


**Fig. 2.** Extended stern angle

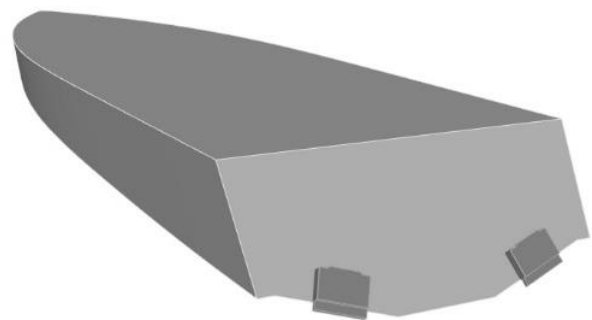


**Fig. 3.** Interceptor installation

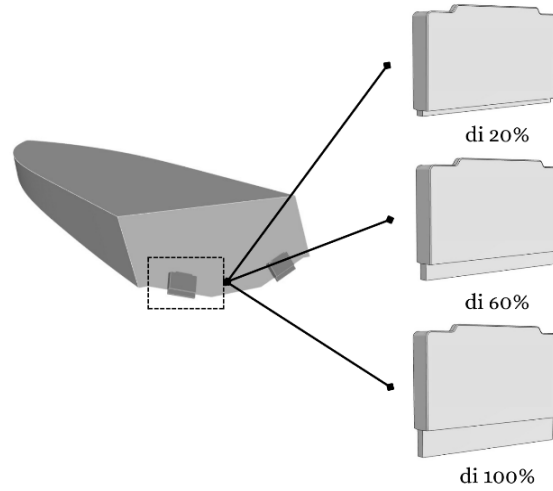


**Fig. 4.** Interceptor height

### 2.3 Numerical Approach

In this study, a method called computational fluid dynamics (CFD) is used to simulate a ship model. The simulation relies on the unsteady Reynolds-Averaged Navier-Stokes equations, a problem-solving approach based on the conservation of mass and momentum principles, to conduct the hydrodynamic simulation [23]. Here is the URANS equation.

$$\frac{\partial U_i}{\partial x_i} = 0 \quad (1)$$

$$\frac{\partial U_i}{\partial t} + \frac{\partial (U_i U_j)}{\partial x_j} = -\frac{1}{\rho} \frac{\partial P}{\partial x_i} + \frac{\partial}{\partial x_i} \left( 2\nu S_{ij} - \overline{u'_i u'_j} \right) \quad (2)$$

Where  $U_i$  and  $u'_i$  express the mean and fluctuation velocity component in the direction of the Cartesian coordinate  $x_i$ ,  $P$  is the mean pressure,  $\rho$  is the density,  $\nu$  is the molecular kinematic viscosity and  $S_{ij}$  is the mean strain-rate tensor. The strain-rate tensor is defined as

$$S_{ij} = \frac{1}{2} \left( \frac{\partial U_i}{\partial x_j} + \frac{\partial U_j}{\partial x_i} \right) \quad (3)$$

The last term on the right-hand side of Eq. (2) is denoted as the Reynolds stress tensor which is given by

$$\tau_{ij} = \overline{u'_i u'_j} = \mu_t \left( \frac{\partial U_i}{\partial x_j} + \frac{\partial U_j}{\partial x_i} - \frac{1}{3} \frac{\partial U_k}{\partial x_k} \delta_{ij} \right) - \frac{2}{3} \rho k \delta_{ij} \quad (4)$$

The Boussinesq (eddy-viscosity) hypothesis obtained with the  $k - \varepsilon$  turbulence model is expressed by

$$\mu_t = \frac{1}{2} \frac{\rho \tau_{ij}}{S_{ij}} \quad (5)$$

The k-ε turbulence model specifies that the turbulent eddy viscosity is calculated by

$$\mu_t = c_\mu \rho \frac{k^2}{\varepsilon} \quad (6)$$

The turbulent kinetic energy  $k$  and the rate of dissipation of the turbulent energy  $\varepsilon$  are calculated below

$$\frac{\partial \rho k}{\partial t} + \frac{\partial \rho U_j k}{\partial x_j} = \frac{\partial}{\partial x_j} \left[ \left( \mu + \frac{\mu_t}{\sigma_t} \right) \frac{\partial k}{\partial x_j} \right] + P_k - \rho \varepsilon \quad (7)$$

$$\frac{\partial \rho \varepsilon}{\partial t} + \frac{\partial \rho U_j \varepsilon}{\partial x_j} = \frac{\partial}{\partial x_j} \left[ \left( \mu + \frac{\mu_t}{\sigma_\varepsilon} \right) \frac{\partial \varepsilon}{\partial x_j} \right] + \frac{\varepsilon}{k} (c_{\varepsilon 1} P_k - c_{\varepsilon 2} \rho \varepsilon) \quad (8)$$

When the energy dissipation rate  $\varepsilon$  and the kinetic energy  $k$  are combined, the turbulent viscosity  $\mu_t$  may be determined. A near-wall function employs a realistic two-layer turbulence technique (k-ε model) to depict the velocity profile close to the wall. In this calculation, the time-step is determined based on the ITTC guideline [24]. At the interface between the phases of water and air, the Volume of Fluid (VOF) approach was used to simulate changes in the free surface. [25]. The time step ( $\Delta t$ ) used in the unsteady simulation should be small enough to complete the motion on a free surface. The time step is the period interval for each iteration calculation. The time step used for this simulation was a function of the ship's speed ( $V$ ) and waterline length ( $L$ ) according to Eq. (9), as recommended by the ITTC. Determining the time step in this research depended on the Courant-Friedrichs-Lewy (CFL) number. The fluid particles' total number of points traveled throughout the interval was denoted by the CFL number. The time step used is smaller for faster ships. This research took the average time step value at 0.008, shown in Figure 5.

$$\Delta t_{ITTC} = 0.005 \sim 0.01 \frac{L}{V} \quad (9)$$

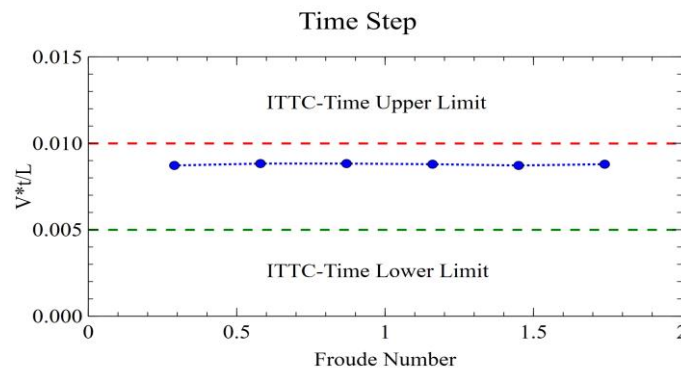


Fig. 5. Time step illustration

Prism layers were made close to the hull to capture the boundary layer's flow accurately, and six prism layers were employed in this research.  $Y^+$  is defined as the non-dimensional distance of the first grid node from the wall surface, normalized by the local viscous length scale. ITTC recommends that the  $Y^+$  value is  $30 < Y^+ < 100$  [24]. It is calculated using Eq. (10). Figure 6 shows  $y^+$  values on ships, where the average  $y^+$  values are 50-100 at  $Fr$  1.45. At the interface between the phases of water and air, the Volume of Fluid (VOF) approach was used to simulate changes in the free surface

[25]. However, it should be noted that the  $Y^+$  value needs to be studied to capture the turbulence phenomenon well.

$$Y^+ = \frac{(\rho \cdot U \cdot y)}{\mu} \tag{10}$$

Where  $U$  the friction velocity at the wall is,  $y$  is the distance from the wall to the first grid node, and  $\mu$  is the dynamic viscosity of the fluid.

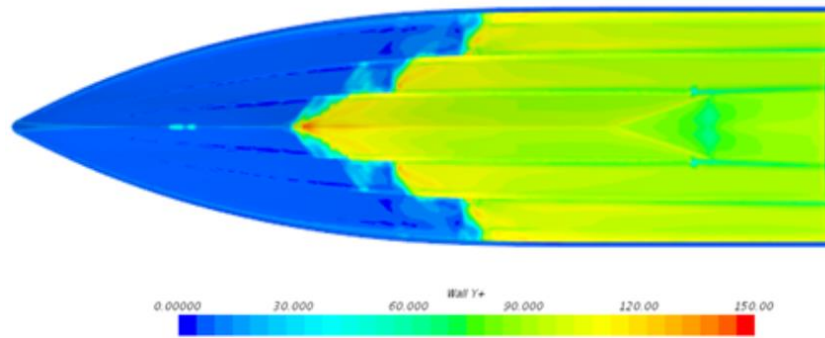


Fig. 6. Wall  $Y^+$  barehull for Fr 1.45

## 2.4 Meshing Strategy

Meshing in this research used the overset mesh method. The overset mesh is a technique that involves the use of donor-acceptor cells. The study considered two geometries: the background served as the donor, while the overset served as the donor recipient. Overset grid is more accurate than other discrete methods such as morphing grid and moving grid. Research by De Luca *et al.*, in 2016 compared the overset grid and moving grid methods. The result reported that the overset grid indicated better results than the moving grid [26]. De Marco *et al.*, compared the overset grid method with the morphing grid. Both revealed good results, but the overset grid was slightly better in predicting the accuracy of the results [27]. Nevertheless, the overset mesh took a long time because the two geometries interacted. The domain size and boundary conditions refer to the ITTC recommendation. The details of the domain size are shown in Table 3, while the boundary conditions are shown in Table 4. Figure 7 illustrates the size of the computational domain and boundary conditions. Based on the length between perpendiculars ( $L$ ), the domain length was measured from  $-2.5 L$  to  $1 L$  with the coordinates of the zero point at the stern and the vessel's draft. The width was set to  $1.5 L$  and the water depth was  $2 L$ . The inflow, bottom, side, and top flow limits were described with inlet velocity; the outlet limits were pressure outlets placed far enough away to ensure no flow reflection occurred, and the fluid could fully expand. The body surface employed a no-slip limit condition. The simulation was carried out on half the hull, it was modeled to save computational time. Normal velocity and gradient variables were zero in the symmetry plane condition.

**Table 3**  
 Computational domain

Parameter	Background	Overset
Length	1L from FP	0.25 from FP
	2.5L from AP	0.25 from AP
Height	1L from deck	0.75H from deck
	2L from keel	0.75 from keel
Breadth	1.5L from symmetry	0.5B from symmetry

**Table 4**  
Boundary conditions

Surface	Boundary conditions
Top	Velocity inlet
Side	Velocity inlet
Bottom	Velocity inlet
Inlet	Velocity inlet
Outlet	Pressure outlet
Symmetry	Symmetry plane
Body	Wall (no slip)

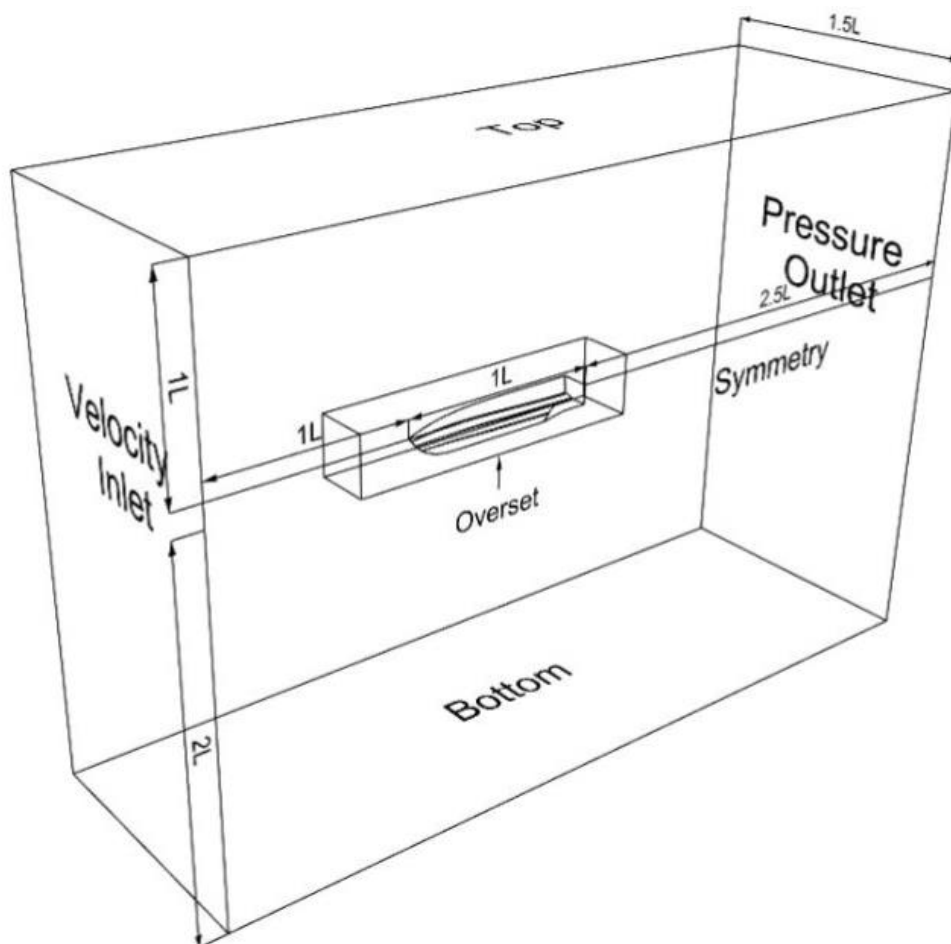


**Fig. 7.** Computational domain and boundary condition

Mesh concentration was measured using isotropic or anisotropic methods based on  $x$ ,  $y$ , and  $z$  coordinates. The denser the mesh concentration would increase the computation time; hence, the mesh density was only carried out in certain parts. Figure 8 demonstrates the concentration of the mesh in specific parts, and the mesh density significantly affects the simulation results.

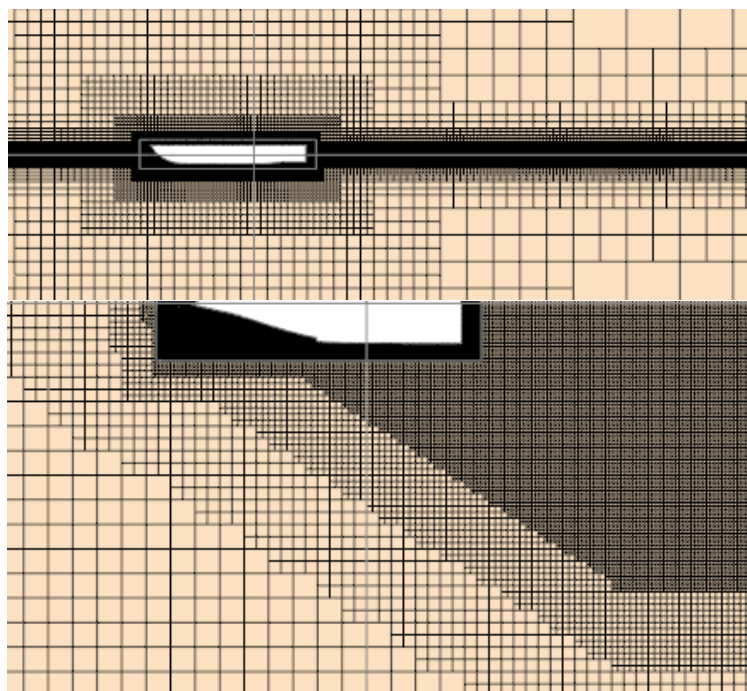


Fig. 8. Mesh density

### 3. Result and Discussion

#### 3.1 Verification of Experiments and CFD

In essence, a model is translated into computer code, enabling the execution of a CFD simulation that generates data utilized in engineering analysis. The process of verification and validation involves scrutinizing both the code and simulation results to identify any errors. Five mesh quantity grids totalling 0.40; 0.69; 1.02; 1.55; and 2.01 in million cells with the Froude number 1.45 shown in Table 5. Resistance is indicated by the non-dimensional  $R/\Delta$ , trim by degree, and heave by the non-dimensional rise of CG/draft units. Ahmed *et al.*, compare experimental and computational results, the results show that the resistance values at various speeds for the fine mesh show a very good and improved agreement with the experimental data, with an error of less than 6% [28]. This indicates that CFD model is capable of simulating the steady flow around a ship hull with an acceptable accuracy and thus can be used as a complementary tool to laboratory model tests for ship design and ship hydrodynamic research [29]. Figure 9 demonstrates that the data obtained was increasingly convergent as the number of meshes increased. The results from grids 4 and 5 indicated good value stability. However, grid 5 required a longer computation time. Therefore, the simulation in this research used grid 4 with a total mesh of 1.55M and a large percentage of error for resistances of 8.89%, 5.97% trim, and 12.97% heave, by still considering the shorter computational time with convergent results.

**Table 5**  
 Total number of mesh

Grid no	Mesh quality	Number of cells
1	Very coarse	404474
2	Coarse	696084
3	Medium	1016192
4	Fine	1550408
5	Very fine	2010230

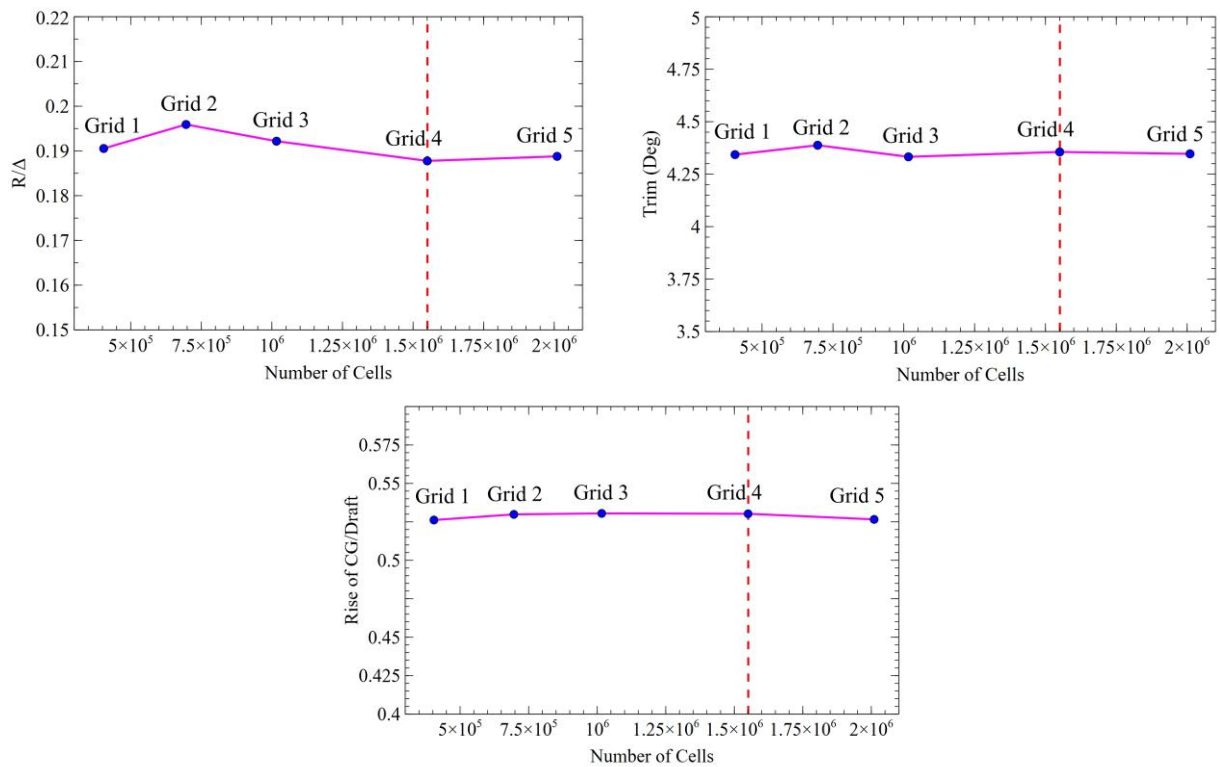


**Fig. 9.** Grid study of drag, trim, and heave

The convergence of model data for resistance, trim, and heave values was evaluated by time, which showed that the data converged after 4 seconds. The convergence of data to time is illustrated in Figure 10.

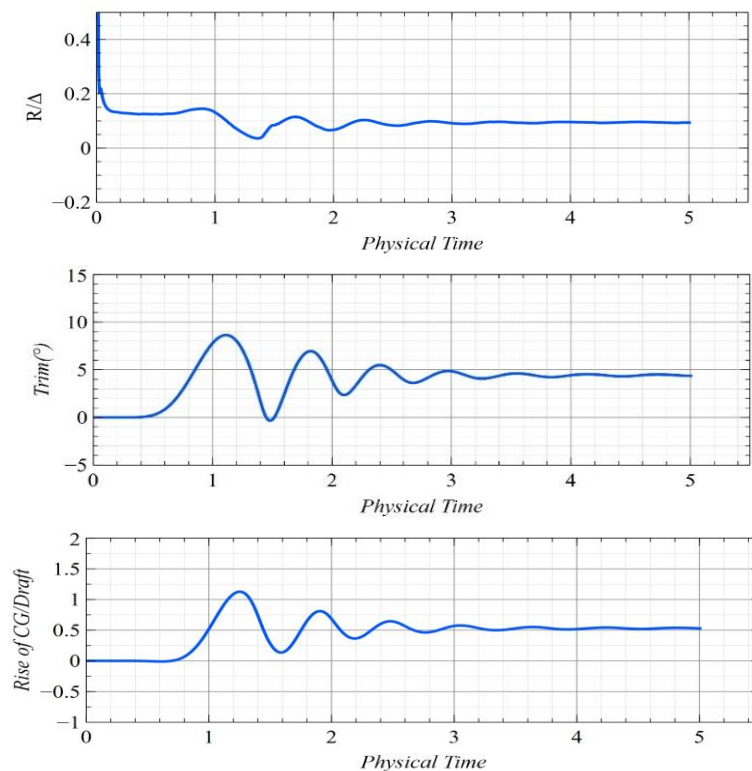


**Fig. 10.** The convergence of hydrodynamics characteristic in time

### 3.2 Validation Process

Figure 11 shows the resistance, trim, and heave results between the experiment and CFD. The pattern's alignment suggested that the numerical simulation findings and the experiment were both reliable. However, calculation gaps/errors were different from the experimental results due to the limitations of numerical simulations in modeling according to actual conditions. Similar cases also occurred in the research by Song *et al.*, with an average error for resistance of 2.65% and trim and sinkage of 9.45% and 7.96% [30]. In this research, there was an average error for resistance of 8.92% and trim and heave, respectively, 3.80% and 12.3% for all speed variations.

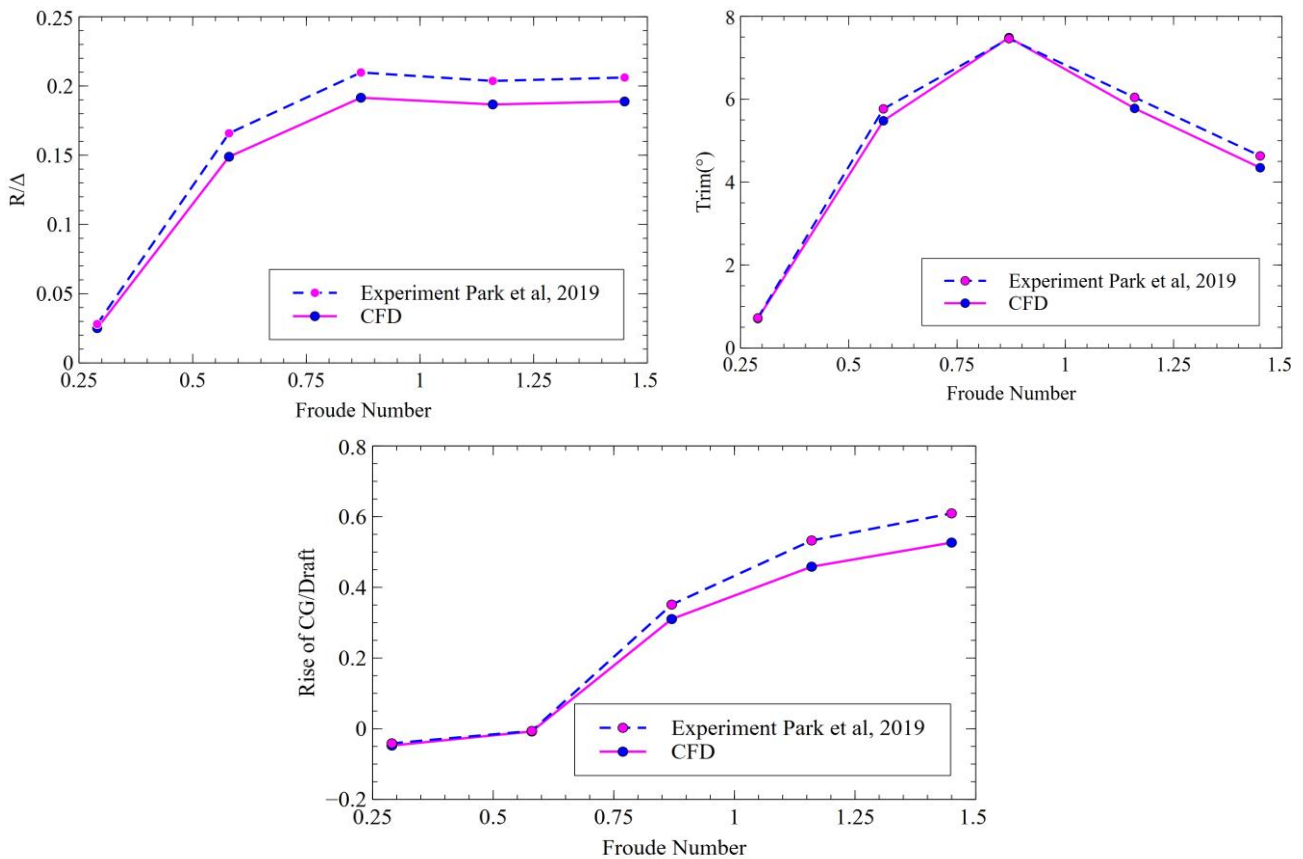


**Fig. 11.** Validation diagram between CFD and experiment

### 3.3 Extended Stern Effect

A ship moving on the water will produce a phenomenon of water flow from the front to the stern. The waves generated as a result of the flow of water hitting the ship's front will pass through the middle of the ship and then go to the ship's rear, which creates a phenomenon of water flow at the ship's rear due to changes in the flow velocity generated from the ship's front. Therefore, the stern hull form's choice also significantly affects the water flow behind the ship. Besides, the determination of the form of the stern hull will significantly affect the magnitude of the resistance value of the ship. Figure 12 shows the reduced resistance, trim, and heave values with different extended stern forms with angles of 10°, 20°, and 30°. The diagram illustrates that the greater the extended stern angle, the greater the effect on the ship's resistance, trim, and heave. The effective reduction occurred at the extended stern angle of 30° Froude number 0.58 with a reduction percentage of 26% resistance,

45% trim, and 20% heave. Extended stern with angles more than 30° is not recommended, as shown on the graph will only add drag at high speeds.

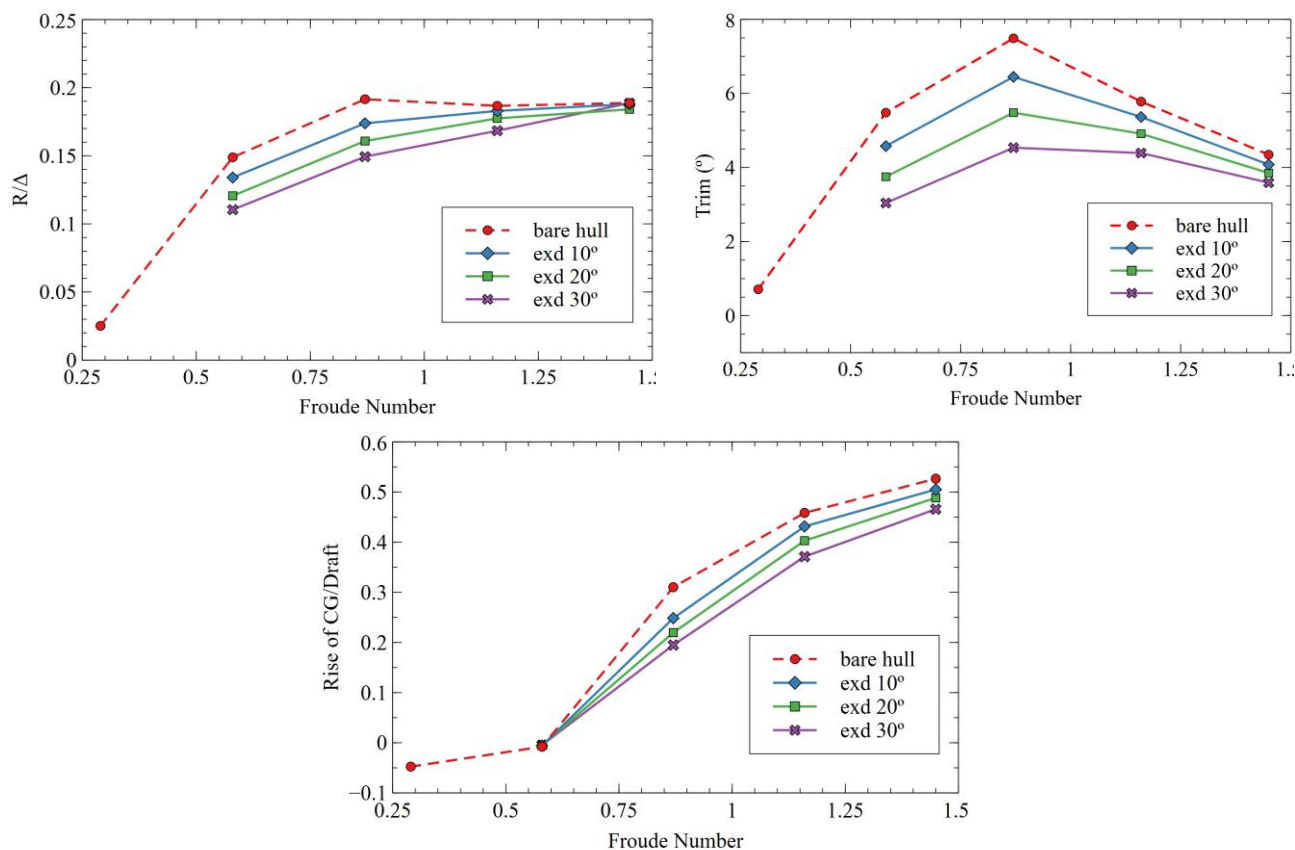


**Fig. 12.** Extended stern effect on drag, trim, and heave

### 3.4 Effect of Interceptor Altitude

The interceptor is a small vertical plate that is usually found close to the stern and runs perpendicular to the hull. The working principle of the interceptor is shown in Figure 13. The main role of the interceptor is to provide a balance between the moment caused by the interceptor and the trim. The increased pressure distribution near the interceptor increased the coefficient of friction and lift. The resulting lift force is greater than the frictional force produced by the interceptor if the interceptor height is properly chosen. The optimal height of the interceptor will increase its efficiency when properly selected [16]. The interceptor's efficiency would be weak, optimal, or equal if the moment it produces is less than, greater than, or equal to the trim moment. The ship's trim will not be properly controlled in a weak interceptor while unfit. The ship's resistance will then increase, causing a negative trim and a safety issue [31]. Therefore, determining the thickness of the ship's transom's boundary layer was the initial stage of designing the interceptor. Figure 14 shows the value of the ship's boundary layer at each speed variation. The boundary layer thickness at transom estimation is based on the water length and speed. An option is CFD, as done in the previous part. However, using CFD to estimate the boundary layer thickness for boats is difficult and time-consuming. Another option is to use an analytical solution as suggested in Ref. [32]. The bottom of the planing boats is almost flat. Thus, as an initial approximation, the boundary layer near the transom (for aft interceptor location) can be considered in the same way as the one over the flat plate having the same length as the hull. The thickness of the boundary layer in turbulent flow can

be calculated [32] via Eq. (11). Where, LWL is the water line length and  $Re_{LWL}$  is the corresponding Reynolds number.

$$h = 0.382 \times LWL / (Re_{LWL})^{0.2} \quad (11)$$

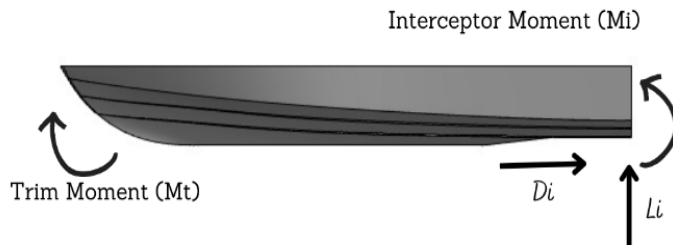


**Fig. 13.** Interceptor working principle

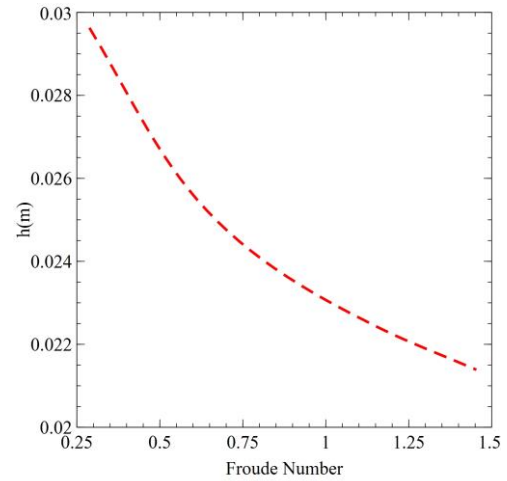


**Fig. 14.** Boundary layer thickness

The interceptor caused considerable changes in pressure around the bottom of the ship, especially on the transoms. Pressure variations affected resistance, draft height, and lift force. Based on recent research, the height of the interceptor should not be higher than 60% ( $d/h \leq 0.6$ ) of the transom boundary layer. For optimal efficiency, when the height of the interceptor is 60% of the boundary layer, the span length of the interceptor must be seven times the height of the interceptor [31]. Considering the variation angles of the interceptor installations, as illustrated in Figure 15, the height of the interceptor ( $d$ ) could be calculated using Eq. (12).

$$d = di \cos \theta \quad (12)$$

Where ( $di$ ) was the interceptor's stroke height, and ( $\theta$ ) was the interceptor's inclination angle. The height comparison of the interceptor and boundary layer ( $d/h$ ) was presented in Figure 16 for each speed variation on resistance and trim. As previously mentioned, when the  $d/h$  ratio was much smaller than 0.6, the efficiency of the interceptor became weak to control trim and reduce resistance. The interceptor would lose effectiveness when  $d/h$  was more significant than 0.6. The interceptor would generate a powerful moment which could create a negative trim. Even worse, it could capsize the ship. To overcome this problem, the height of the interceptor must be reduced. The height of the drop would reduce the lift force and combine the interceptor with a trim tab [33].

In this research, the  $d/h$  value in the range of 0.31 - 0.43 was still satisfactory concerning previous research, which was not more than 0.6. The ratio of the height of the interceptor to the boundary layer ( $d/h$ ) suggested for ships with extended stern  $10^\circ$  was 0.38, while ships with extended stern  $20^\circ$  and  $30^\circ$  were 0.37 and 0.34 respectively, referring to the improvement in the best performance value of the ship on Froude number 0.87. If the  $d/h$  value were too large or exceeded 0.6, it would result in excessive trim and increased resistance, which could cause safety problems.

The effectiveness of the interceptor could be increased by paying attention to the height of the interceptor at each speed. The interceptor, which could be controlled in height when the ship was operating, could increase effectiveness when adjusting to the ship's speed.

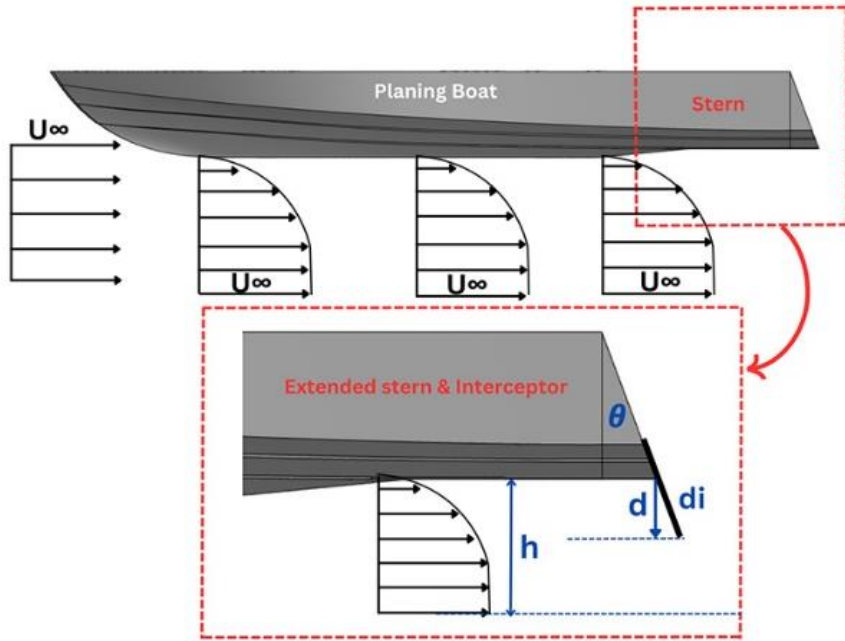


Fig. 15. Comparison of boundary layer thickness and interceptor height

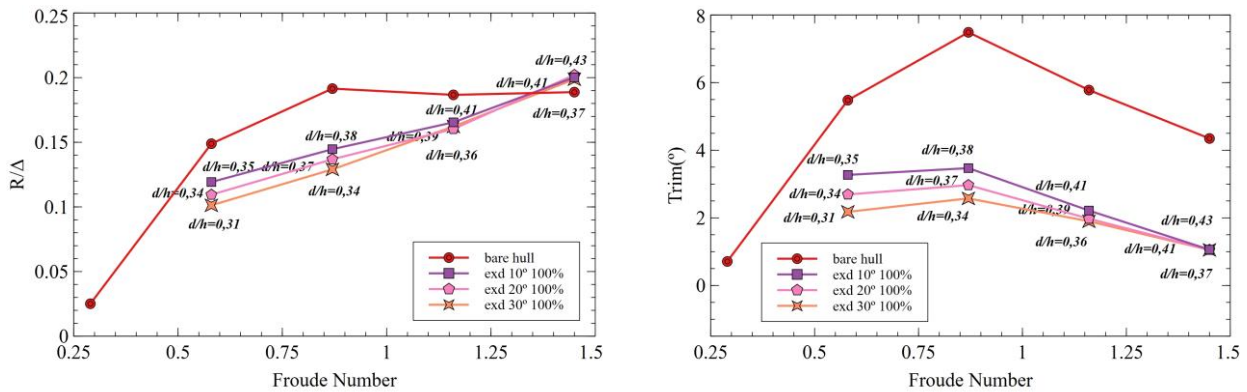


Fig. 16. Boundary layer and interceptor height ratio ( $d/h$ )

The research results are shown in Figure 17 with variations in the extended stern angles of 10°, 20°, and 30° at interceptor height conditions of 100%, 60%, and 20%. Generally, high-speed planing vessels are divided into three phases: the displacement phase, the semi-displacement/ semi-planing phase, and the planing phase. Figure 17 (a) demonstrates the improvement in resistance values in the displacement, semi-displacement/ semi-planing phase, and the planing phase, namely at the Froude number 0.29 to 1.45. However, the best resistance improvement occurred in the semi-displacement phase at Froude number 0.87, with a reduction percentage of 24% extended at 10°, 29% extended at 20°, and 33% extended at 30° with 100% interceptor. Likewise, with the conditions of 60% and 20% interceptor, it had the same pattern as the 100% interceptor; i.e., there was an improvement in the resistance value in the semi-displacement phase. The best resistance value improvement occurred at the Froude number 0.87, with a percentage reduction in resistance values in the 13% to 29% range. However, at Froude number > 1.45, the interceptor was not needed because it would only increase the ship's resistance.

The trim analysis results can be seen in Figure 17 (b). The trim decrease had the same pattern in each variation. The trim value was improved on the Froude number 0.87 with a reduction percentage of 54% extended 10°, 60% extended 20°, and 66% extended 30° at the height of 100% interceptor. As for the height of 60% and 20% improvement, the best trim value was the Froude number 0.87,

with a reduction percentage of 24% to 49%. Trim visualization can be seen in Figure 18 with a significant reduction in trim angle from the bare hull and extended stern variations and the addition of an interceptor at Froude number 0.87. The interceptor was not recommended at high speeds because it would cause excessive trim.

Figure 17 (c) illustrates the heave graph; there were improvements in the heave value with a consistent pattern for each variation and the heave value with a range of 27% to 47%. The best reduction in heave value was 47% at the Froude number 0.87 extended 30° with a height of 100% interceptor. It is similar to the interceptor height of 20% and 60%, with a reduction in the heave value of 38% and 45% at the Froude number 0.87.

The speed and height of the interceptor were essential factors in the effectiveness of the interceptor. Figure 17 (d) shows the lift force at the extended stern angle and interceptor height variation. This research discovered that the lift force due to the interceptor got more significant as the ship's speed increased, but the change was not too significant. The highest increase occurred at the Froude number 1.45 with a percentage of 2.73% at the extended stern 30°, and the interceptor height was 100% with an average lift force of 1.72% at each speed variation.

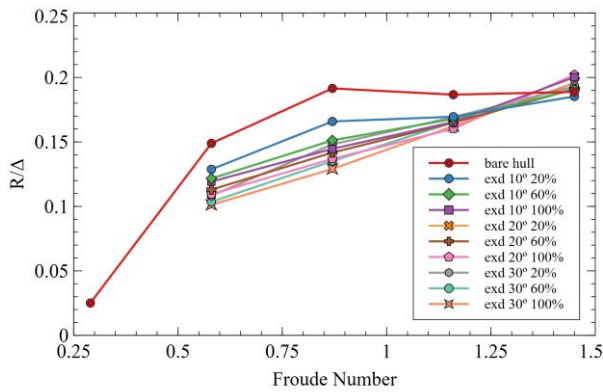


Fig. 17. (a) Drag

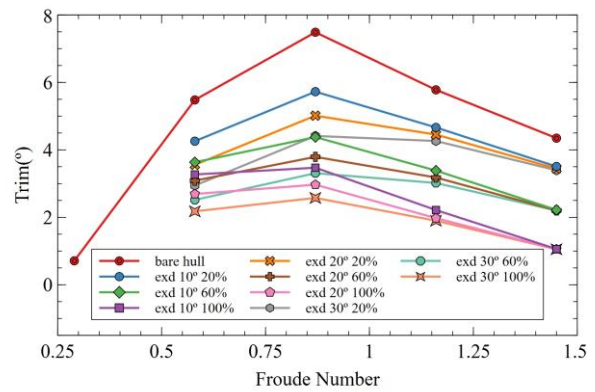


Fig. 17. (b) Trim

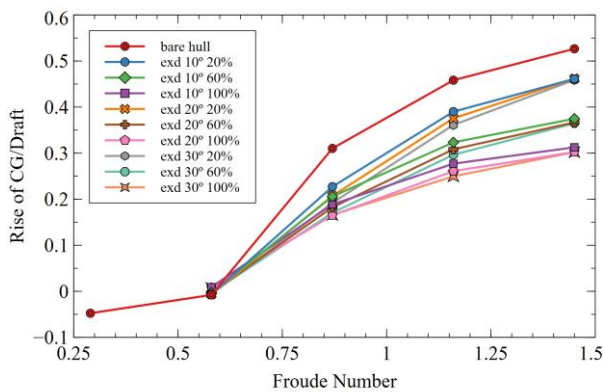


Fig. 17. (c) Heave

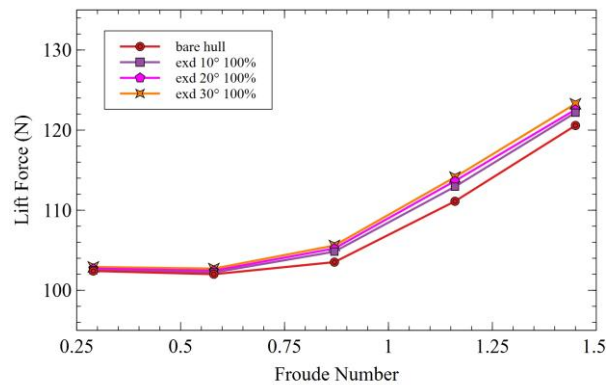
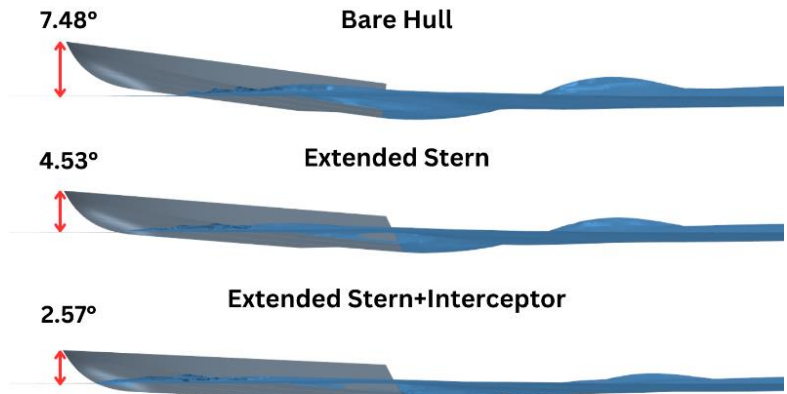
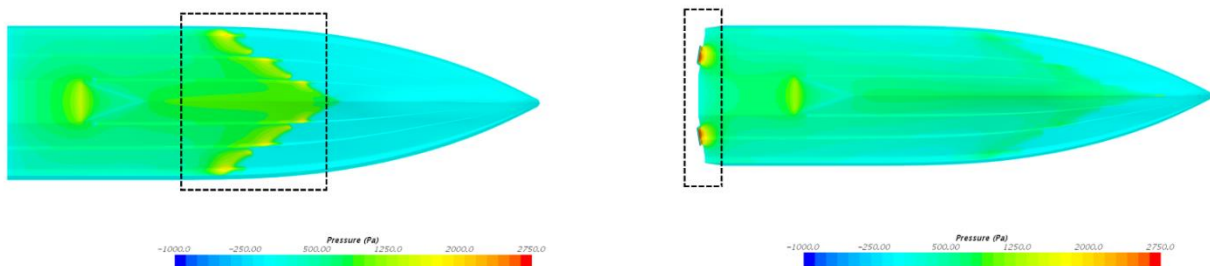


Fig. 17. (d) Lift force



**Fig. 18.** Reduced trim due to interceptor on Fr 0.87

The pressure distribution at the bottom of the ship in the bare hull and extended stern conditions using the interceptor is illustrated in Figure 19. The pressure in the transom for the hull without the interceptor was observed to be less than employing the interceptor. The pressure distribution decreased from the high-pressure area in the bow to the stern where the interceptor had been installed. It created an interceptor moment, which would affect trim. The moment triggered was due to the presence of a flowing fluid that was restrained by the interceptor and caused pressure. This pressure creates an upward lift and reduces trim. The optimal interceptor was obtained when the interceptor moment was equal to the trim moment.



**Fig. 19.** Pressure distribution of the bare hull and the interceptor at the bottom

Figure 20 shows the wave pattern on the free surface behind the ship's stern at Froude number 0.87. It revealed that the pressure value near the ship's stern increased with the presence of an interceptor, which caused the wave pool formed behind the ship's stern to divide into two. It caused a reduction in the ship's resistance value and trim value. A similar case was observed for other fraud numbers where an interceptor was useful.

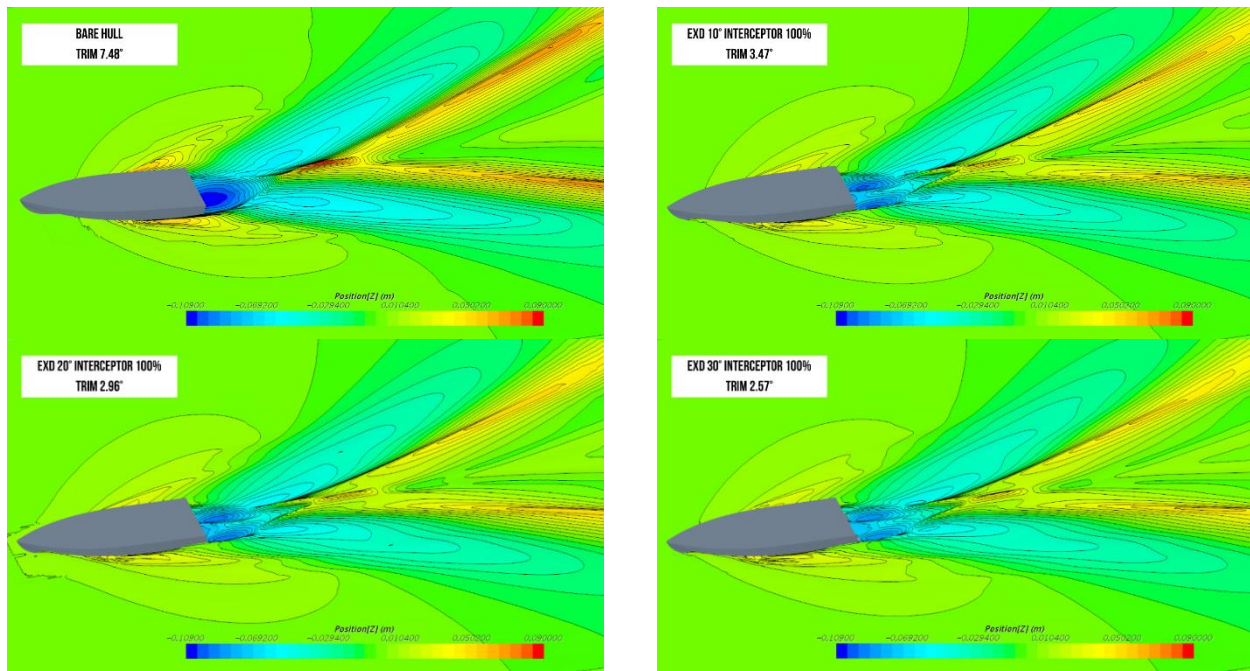


Fig. 20. Wave pattern at the stern

#### 4. Conclusions

In this research, the effect of the extended stern form with different angles and the variation of the height of the interceptor at various speeds was investigated. The conclusions obtained are as follows:

- i. The extended stern form without an interceptor could affect the ship's resistance, trim, and heave values. This research revealed that the more significant the stern extend angle, the greater the reduction in resistance in the semi-displacement phase. The effective reduction occurred at the Froude number 0.58 to 0.87 with a percentage reduction in the resistance value of 26% extended stern 30°. However, the resistance increased at high speeds as the extended stern angle increased.
- ii. Adding an interceptor on the extended stern significantly reduced resistance, trim, and heave values. The effective reduction occurred in the semi-displacement phase, namely at the Froude number 0.58 to 0.87, with a percentage reduction in the resistance value of 33%, and trim and heave were 66% and 47% for the extended stern 30° with an interceptor height of 100%.
- iii. Using an interceptor at high speed was not recommended, or the Froude number was more than 1.45 because it would increase the ship's resistance and cause excessive trim that could endanger safety.
- iv. The recommended ratio of boundary layer and interceptor height ( $d/h$ ) on ships with extended stern 10°, 20°, and 30° were 0.38, 0.37, and 0.34 at Froude number 0.87.

#### Acknowledgement

The authors gratefully acknowledge financial support from Universitas Diponegoro for this work under the project scheme of Riset Publikasi Internasional (RPI) No. 259/UN7.A/HK/VIII/2023.

## References

- [1] Karimi, Mohammad Hossein, Mohammad Saeed Seif, and Majid Abbaspoor. "A study on vertical motions of high-speed planing boats with automatically controlled stern interceptors in calm water and head waves." *Ships and Offshore Structures* 10, no. 3 (2015): 335-348. <https://doi.org/10.1080/17445302.2013.867647>
- [2] Park, Jong-Yong, Hujae Choi, Jooho Lee, Hwiyoung Choi, Joohyun Woo, Seonhong Kim, Dong Jin Kim, Sun Young Kim, and Nakwan Kim. "An experimental study on vertical motion control of a high-speed planing vessel using a controllable interceptor in waves." *Ocean Engineering* 173 (2019): 841-850. <https://doi.org/10.1016/j.oceaneng.2019.01.019>
- [3] Seok, Woochan, Sae Yong Park, and Shin Hyung Rhee. "An experimental study on the stern bottom pressure distribution of a high-speed planing vessel with and without interceptors." *International Journal of Naval Architecture and Ocean Engineering* 12 (2020): 691-698. <https://doi.org/10.1016/j.ijnaoe.2020.08.003>
- [4] Tsai, J. F., and J. L. Hwang. "Study on the compound effects of interceptor with stern flap for two fast monohulls." In *Oceans' 04 MTS/IEEE Techno-Ocean'04 (IEEE Cat. No. 04CH37600)*, vol. 2, pp. 1023-1028. IEEE, 2004.
- [5] Fitriadhy, Ahmad, Intan Nur Nabila, Christina Bangi Grosnin, Faisal Mahmuddin, and Suandar Baso. "Computational Investigation into Prediction of Lift Force and Resistance of a Hydrofoil Ship." *CFD Letters* 14, no. 4 (2022): 51-66. <https://doi.org/10.37934/cfdl.14.4.5166>
- [6] Day, Alexander H., and Christopher Cooper. "An experimental study of interceptors for drag reduction on high-performance sailing yachts." *Ocean Engineering* 38, no. 8-9 (2011): 983-994. <https://doi.org/10.1016/j.oceaneng.2011.03.006>
- [7] Ghassemi, H., M. Mansouri, and S. Zaferanlouei. "Interceptor hydrodynamic analysis for handling trim control problems in the high-speed crafts." *Proceedings of the Institution of Mechanical Engineers, Part C: Journal of Mechanical Engineering Science* 225, no. 11 (2011): 2597-2618. <https://doi.org/10.1177/0954406211406650>
- [8] Suneela, J., P. Krishnankutty, and V. Anantha Subramanian. "Numerical investigation on the hydrodynamic performance of high-speed planing hull with transom interceptor." *Ships and Offshore Structures* 15, no. sup1 (2020): S134-S142. <https://doi.org/10.1080/17445302.2020.1738134>
- [9] Sahin, Omer Sinan, Emre Kahramanoglu, and Ferdi Cakici. "Numerical evaluation on the effects of interceptor layout and blade heights for a prismatic planing hull." *Applied Ocean Research* 127 (2022): 103302. <https://doi.org/10.1016/j.apor.2022.103302>
- [10] Karimi, Mohammad Hosein, Mohammad Saeed Seif, and Madjid Abbaspoor. "An experimental study of interceptor's effectiveness on hydrodynamic performance of high-speed planing crafts." *Polish maritime research* 20, no. 2 (2013): 21-29. <https://doi.org/10.2478/pomr-2013-0013>
- [11] Kim, Dong Jin, Sun Young Kim, Young Jun You, Key Pyo Rhee, Seong Hwan Kim, and Yeon Gyu Kim. "Design of high-speed planing hulls for the improvement of resistance and seakeeping performance." *International Journal of Naval Architecture and Ocean Engineering* 5, no. 1 (2013): 161-177. <https://doi.org/10.2478/IJNAOE-2013-0124>
- [12] Mansoori, Mehran, and Antonio Carlos Fernandes. "The interceptor hydrodynamic analysis for controlling the porpoising instability in high speed crafts." *Applied Ocean Research* 57 (2016): 40-51. <https://doi.org/10.1016/j.apor.2016.02.006>
- [13] Suneela, Jangam, and Prasanta Sahoo. "Numerical investigation of interceptor effect on seakeeping behaviour of planing hull advancing in regular head waves." *Brodogradnja: Teorija i praksa brodogradnje i pomorske tehnike* 72, no. 2 (2021): 73-92. <https://doi.org/10.21278/brod72205>
- [14] Samuel, S., Ocid Mursid, Serliana Yulianti, Kiryanto Kiryanto, and Muhammad Iqbal. "Evaluation of interceptor design to reduce drag on planing hull." *Brodogradnja: Teorija i praksa brodogradnje i pomorske tehnike* 73, no. 3 (2022): 93-110. <https://doi.org/10.21278/brod73306>
- [15] Samuel, S., Serliana Yulianti, Parlindungan Manik, and Abubakar Fathuddiin. "A study of interceptor performance for deep-v planing hull." In *IOP Conference Series: Earth and Environmental Science*, vol. 1081, no. 1, p. 012004. IOP Publishing, 2022. <https://doi.org/10.1088/1755-1315/1081/1/012004>
- [16] Mansoori, M., and A. C. Fernandes. "Hydrodynamics of the interceptor on a 2-D flat plate by CFD and experiments." *Journal of Hydrodynamics, Ser. B* 27, no. 6 (2015): 919-933. [https://doi.org/10.1016/S1001-6058\(15\)60555-8](https://doi.org/10.1016/S1001-6058(15)60555-8)
- [17] Yousefi, Reza, Rouzbeh Shafaghat, and Mostafa Shakeri. "Hydrodynamic analysis techniques for high-speed planing hulls." *Applied ocean research* 42 (2013): 105-113. <https://doi.org/10.1016/j.apor.2013.05.004>
- [18] Sukas, Omer Faruk, Omer Kemal Kinaci, Ferdi Cakici, and Metin Kemal Gokce. "Hydrodynamic assessment of planing hulls using overset grids." *Applied Ocean Research* 65 (2017): 35-46. <https://doi.org/10.1016/j.apor.2017.03.015>

- [19] Fathuddiin, Abubakar, Samuel Samuel, Kiryanto Kiryanto, and Aulia Widyandari. "Prediksi hambatan kapal dengan menggunakan metode overset mesh pada kapal planing hull." *Rekayasa Hijau: Jurnal Teknologi Ramah Lingkungan* 4, no. 1 (2020): 24-34. <https://doi.org/10.26760/jrh.v4i1.24-34>
- [20] D. J. Kim, and S. Y. Kim. "Comparative study on manoeuvring performance of model and full-scale waterjet propelled planing boats." Society of Naval Architects and Marine Engineers (SNAME), 2017.
- [21] Kim, Dong Jin, and Sun Young Kim. "Turning characteristics of waterjet propelled planing boat at semi-planing speeds." *Ocean Engineering* 143 (2017): 24-33. <https://doi.org/10.1016/j.oceaneng.2017.07.034>
- [22] Humphree, "Interceptors Series," 2022. [Online]. Available: <https://humphree.com/>. [Accessed: 02-Aug-2021].
- [23] Kinaci, Omer K., Omer F. Sukas, and Sakir Bal. "Prediction of wave resistance by a Reynolds-averaged Navier–Stokes equation–based computational fluid dynamics approach." *Proceedings of the Institution of Mechanical Engineers, Part M: Journal of Engineering for the Maritime Environment* 230, no. 3 (2016): 531-548. <https://doi.org/10.1177/1475090215599>
- [24] ITTC Specialist Committee. "Recommended procedures and guidelines-Practical Guidelines for Ship CFD Applications." In *26th International Towing Tank Conference, Rio de Janeiro, Brasil*. 2011.
- [25] Suneela, J., P. Krishnankutty, and V. Anantha Subramanian. "Hydrodynamic performance of planing craft with interceptor-flap hybrid combination." *Journal of Ocean Engineering and Marine Energy* 7 (2021): 421-438. <https://doi.org/10.1007/s40722-021-00211-0>
- [26] De Luca, Fabio, Simone Mancini, Salvatore Miranda, and Claudio Pensa. "An extended verification and validation study of CFD simulations for planing hulls." *Journal of Ship Research* 60, no. 02 (2016): 101-118. <https://doi.org/10.5957/jsr.2016.60.2.101>
- [27] De Marco, Agostino, Simone Mancini, Salvatore Miranda, Raffaele Scognamiglio, and Luigi Vitiello. "Experimental and numerical hydrodynamic analysis of a stepped planing hull." *Applied Ocean Research* 64 (2017): 135-154. <https://doi.org/10.1016/j.apor.2017.02.004>
- [28] Elhadad, Alaaeldeen M., and Abo El-Ela. "Experimental and Cfd Resistance Validation of Naval Combatant Dtm 5415 Model." *Experimental and Cfd Resistance Validation of Naval Combatant Dtm 5415*. <https://doi.org/10.37934/arfmts.107.2.84102>
- [29] Ahmed, Alaaeldeen Mohamed Elhadad. "Comparative investigation of resistance prediction for surface combatant ship model using CFD modeling." *Journal of Advanced Research in Fluid Mechanics and Thermal Sciences* 107, no. 2 (2023): 225-235. <https://doi.org/10.37934/arfmts.107.2.225235>
- [30] Song, Ke-wei, Chun-yu Guo, Jie Gong, Ping Li, and Lian-zhou Wang. "Influence of interceptors, stern flaps, and their combinations on the hydrodynamic performance of a deep-vee ship." *Ocean Engineering* 170 (2018): 306-320. <https://doi.org/10.1016/j.oceaneng.2018.10.048>
- [31] Mansoori, M., A. C. Fernandes, and H. Ghassemi. "Interceptor design for optimum trim control and minimum resistance of planing boats." *Applied Ocean Research* 69 (2017): 100-115. <https://doi.org/10.1016/j.apor.2017.10.006>
- [32] Schlichting, Hermann, and Joseph Kestin. *Boundary layer theory*. Vol. 121. New York: McGraw-Hill, 1961.
- [33] Mansoori, M., and A. C. Fernandes. "Interceptor and trim tab combination to prevent interceptor's unfit effects." *Ocean engineering* 134 (2017): 140-156. <https://doi.org/10.1016/j.oceaneng.2017.02.024>